HHS Public Access

Author manuscript

Nano Today. Author manuscript; available in PMC 2023 April 07.

Published in final edited form as:

Nano Today. 2022 August ; 45: . doi:10.1016/j.nantod.2022.101515.

Nanopore-based disease diagnosis using pathogen-derived tryptic peptides from serum

Wenshu Zheng[a,b], **Julian G. Saliba**[a,c], **Xiaojun Wei**[d,e], **Qingbo Shu**[a,b], **Lane M. Pierson**[a,b], **Liyan Mao**[a,b], **Chang Liu**[d,e], **Christopher J. Lyon**[a,b], **Chen-Zhong Li**[a,b], **William C. Wimley**[b], **Tony Ye Hu**[a,b,*]

[a]Center for Cellular and Molecular Diagnostics, Tulane University School of Medicine, New Orleans, LA, USA

[b]Department of Biochemistry and Molecular Biology, Tulane University School of Medicine, New Orleans, LA, USA

[c]Department of Biomedical Engineering, Tulane University School of Science & Engineering, New Orleans, LA, USA

[d]Biomedical Engineering Program, University of South Carolina, Columbia, SC 29208, USA

[e]Department of Chemical Engineering, University of South Carolina, Columbia, SC 29208, USA

Abstract

Nanopore sensors have shown great utility in nucleic acid detection and sequencing approaches. Recent studies also indicate that current signatures produced by peptide-nanopore interactions can distinguish high purity peptide mixtures, but the utility of nanopore sensors in clinical applications still needs to be explored due to the inherent complexity of clinical specimens. To fill this gap between research and clinical nanopore applications, we describe a methodology to select peptide biomarkers suitable for use in an immunoprecipitation-coupled nanopore (IP-NP) assay, based on their pathogen specificity, antigenicity, charge, water solubility and ability to produce a characteristic nanopore interaction signature. Using tuberculosis as a proof-of-principle example in a disease that can be challenging to diagnose, we demonstrate that a peptide identified by this approach produced high-affinity antibodies and yielded a characteristic peptide signature that was detectable over a broad linear range, to detect and quantify a pathogen-derived peptide

*Corresponding author at: Center for Cellular and Molecular Diagnostics, Tulane University School of Medicine, New Orleans, Louisiana, USA. tonyhu@tulane.edu (T.Y. Hu).

Declaration of Competing Interest

The authors declare that they have no known competing financial interests or personal relationships that could have appeared to influence the work reported in this paper.

CRediT authorship contribution statement

Wenshu Zheng: Conceptualization, Methodology, Validation, Writing – original draft. **Julian G. Saliba:** Conceptualization, Methodology, Validation, Writing – original draft. **Qingbo Shu:** Methodology, Investigation. **Xiaojun Wei:** Methodology, Investigation. **Lane M. Pierson:** Methodology, Investigation. **Liyan Mao:** Methodology, Investigation. **Chang Liu:** Methodology, Investigation. **William C. Wimley:** Methodology, Investigation. **Chen-Zhong Li**: Investigation, Writing – original draft. **Christopher J. Lyon:** Conceptualization, Writing, Investigation. **Tony Ye Hu:** Conceptualization, Methodology, Writing, Funding acquisition.

Appendix A. Supporting information

Supplementary data associated with this article can be found in the online version at doi:10.1016/j.nantod.2022.101515.

from digested human serum samples with high sensitivity and specificity. This nanopore signal distinguished serum from a TB case, non-disease controls, and from a TB-case after extended anti-TB treatment. We believe this assay approach should be readily adaptable to other infectious and chronic diseases that can be diagnosed by peptide biomarkers.

Keywords

Nanopore; Peptide biomarkers; Infectious diseases; Blood tests

Introduction

Traditional immunoassay applications widely employed to detect biomarker proteins usually cannot distinguish proteins that contain minor sequence variations, or specific variant peptides of these proteins, due to multiple technical issues [1–3]. This can be a significant problem when it is necessary to distinguish between biomarkers of related pathogens, which may exhibit substantial protein conservation. Specific antibodies that can distinguish minor sequence variations must recognize, with high affinity, an accessible surface region that contains a species-specific amino acid conformation. However, it is not possible to selectively produce antibodies to such regions in intact proteins or easily select those that bind to these regions among the overall antibody population induced by an intact protein. Even if such antibodies could be generated, their binding sites might be masked by antibodies produced by the host immune response to reduce the detection of these proteins. Minor peptide sequence differences can distinguish proteins that exhibit substantial overall sequence conservation, however, and serve as biomarkers to distinguish closely related organisms, including different closely related members of pathogen superfamilies [4,5]. It is also simple to generate antibodies to such peptides, and these peptides should not be masked by host antibodies since the sample digestion that produces these target peptides should cleavage the host antibodies and disrupt immune complexes to attenuate the potential for antibody competition. Peptide biomarkers are thus good candidates for disease-specific biomarkers, and may be useful in differentiating related pathogens that produce similar symptoms but require different therapeutic interventions for effective disease treatment. Similar peptide differences can be used to distinguish mutant proteins associated with cancer [6,7]. Specific detection of such peptide variants can thus provide the most accurate protein-level evidence to distinguish infections caused by specific members of a pathogen family or to detect the presence of specific mutations, and be applied to applications targeting infectious disease and cancer [8–11].

Specific antibodies can be directly raised against variant peptide regions of interest but such peptide-specific antibodies may cross-react with other peptides produced upon digestion of complex biological samples since short peptides often do not demonstrate tertiary topological structures that promote specific interaction of an antibody with its target epitope [1,2,12]. Furthermore, these peptides are often not suitable for use in standard sandwich immunoassays since they may be too short to contain two non-inferring antibody epitopes. Mass spectrometry is the gold-standard method for peptide identification, as mass-to-charge ratios detected for target proteins and their fragmentation ions can directly indicate their

amino acid sequence. However, this approach is labor-intensive and utilizes expensive equipment that requires significant infrastructure support and highly-trained personnel to obtain sensitive and accurate results, and thus is not feasible for use in remote and resource-limited clinical settings in low to middle-income countries where several major infectious diseases are often prevalent [13–15].

Nanopore-based sensors have been extensively utilized in ultra-sensitive detection of specific nucleic acid targets, and may also represent an inexpensive potential alternative to mass spectrometry for high-specificity identification and quantification of biomarker peptide variants [16]. Nanopores produce characteristic ion currents in response to a specific applied voltage, pH and salt concentrations, and these currents are very sensitive to interactions with molecules that can block, occupy, or translocate through their ion channels and generate current versus time signature profiles that can be specific for a given target molecule [17,18]. Such interactions can be highly specific, to the extent that nanopore current signatures produced during the transit of single-stranded RNA and DNA oligonucleotides have been utilized to develop nanopore-based sequencing applications [19,20]. Recent studies have indicated that current signatures produced by peptide-nanopore interactions can distinguish polymeric peptides of different lengths or that differ by a single amino acid [21–24], although the greater sequence, electrochemical, and conformational complexity of peptides renders them unsuitable for direct sequencing applications. Nanopore research directed at protein discrimination has thus primarily focused on applications that can detect specific proteins as a result of a change in the characteristic nanopore signal of aptamers that form specific interactions with these proteins [25], or the detection of structural dynamic properties that can distinguish unrelated proteins or conformational changes in select proteins upon co-factor or ligand binding events [26,27]. However, key studies have demonstrated the ability of signals produced by peptide-nanopore interactions to analyze peptide/protein processes, including protein unfolding, peptide modification, and multiplex detection of peptides [21,28–31], showing the great potential of nanopore-based peptide analysis from clinical specimens. However, these studies primarily employ high purity samples and appear to be incompatible with the high sample complexity encountered in standard clinical specimens.

New approaches are therefore needed to select peptides suitable for use as diagnostic markers in nanopore assays and to detect signals produced by these targets against an expected high background of non-specific peptide signals present in complex biological samples used for clinical diagnoses. We therefore developed a methodology to identify peptides that could serve as nanopore-read biomarkers based on their pathogen specificity, antigenicity, charge, water solubility, and nanopore signal characteristics, and used an immunoprecipitation-coupled nanopore (IP-NP) sensor to specifically detect and quantify these candidate biomarker peptides after their enrichment from trypsin-digested serum samples (Scheme 1). In this approach, peptide-specific IP of target peptides should greatly reduce non-specific background, while characteristic current signatures produced upon target peptide interaction with the nanopore should permit its specific detection and quantification. We evaluated the ability of this approach to identify and detect target peptides derived from two *Mycobacterium tuberculosis* (*Mtb*) virulence factors in serum, since we have previously shown that serum levels of these proteins can identify individuals with

tuberculosis (TB) [32], a leading cause of death from infectious disease [33], including individuals with culture-negative TB who cannot be directly diagnosed with current assays [34]. We herein report that an IP-NP assay can detect an *Mtb*-specific peptide in trypsin-digested serum to permit TB diagnosis.

Results and discussion

Selection of Mtb-specific peptides as biomarkers for nanopore-based TB diagnosis

A peptide biomarker detected in a serum-based nanopore assay for TB diagnosis, should meet three key criteria: 1) it should derive from an *Mtb* protein associated with active versus latent TB infection; 2) it should demonstrate sufficient antigenicity to permit specific high-affinity enrichment from digested serum samples; and 3) it should be water-soluble, have a net positive or negative charge, and produce a characteristic nanopore interaction signal, which should exhibit a high association rate constant (K_{on}). The *Mtb* virulence factors 10 kDa culture filtrate protein (CFP-10) and 6 kDa early secretory antigen target (ESAT-6) represent good candidates for TB biomarkers since they are actively secreted by all virulent *Mtb* strains, and transfer of their gene locus to attenuated *Mtb* strains increases the survival and virulence of these strains [35]. ESAT-6 and CFP10 are likely to form immune complexes in the circulation, but we have reported that peptides derived from both proteins can be detected in trypsin digested serum of TB patients by an IP-coupled mass spectrometry assay, and their detection had good performance to diagnose all manifestations of TB in various affected patient populations [36]. We therefore evaluated the potential utility of all tryptic peptides produced by these two proteins.

Sequence analysis of these two virulence factors indicated that CFP-10 can produce seven tryptic peptides with ≥ 7 amino acids that could serve as potential antibody targets for IP-based enrichment, while analysis of ESAT-6 identified four peptides with the potential to function in this manner (Fig. 1a). Bioinformatic analysis indicated the first CFP-10 peptide (C1) and the second and fourth ESAT-6 peptides (E2 and E4) had predicted antigenicity scores > 1 and therefore reached the threshold for good peptide antigen candidates (Fig. 1b), but only C1 and E4 revealed overall net charge, and only C1 revealed good predicted solubility to meet all three criteria for a good nanopore readout target (Fig. 1b–c; details for charge and solubility analyses are presented in SI methods). The C1 circular dichroism spectra did not reveal obvious differences or evidence of any organized secondary structure under a variety of high salt concentrations used as recording solutions for nanopore measurements, since all spectral curves detected in these solutions were within the range expected for random coils (Fig. S1). Monoclonal antibodies generated against the C1 peptide (CFP10pep hereafter) demonstrated variable affinity for this target upon analysis by indirect ELISA, and the 10A5 clone was selected for all subsequent experiments due to its superior signal-to-noise ratio when employed to detect low abundance CFP10pep target (Fig. 1d–e) [37]. This antibody did not exhibit obvious cross-reactivity with peptides generated upon trypsin digest of a pooled healthy human serum sample, or high concentrations of several peptides liberated by trypsin digestion of other *Mtb* proteins (MPT64, ESAT6, Ag85b, LpqH, and Ag85a), or proteins of other pathogens (Hepatitis B core protein, Influenza A HA protein, and the SARS-CoV-2 S protein) (Fig. 1f).

CFP10pep detection via characteristic αHL signals

Nanopore interactions with peptides can also distinguish different peptides as short-lived resistive pulses that occur when different peptides interact with a nanopore can differ based on their chemical and structural properties to produce characteristic current interruptions that exhibit differential dwell times (t_{off}) due to differences in the extent of their interactions with the nanopore (Fig. 2a) [38]. Studies have shown that peptides with different charges can be discriminated in the nanopore when these peptides are detected from the *trans* side [39]. We therefore evaluated nanopore signals produced when each of these peptides was added to the *trans* well of αHL nanopore chamber at neutral pH, using a voltage potential was used to drive anions from the *trans* to *cis* chamber and vice versa (Fig. S2).

Synthetic CFP10pep preferentially interacts with the αHL nanopore *trans* face at neutral pH, as indicated by differential rates of short-lived resistive pulses when CFP10pep was added the *trans* versus *cis* side of the nanopore chamber (Fig. S3), through a process we hypothesize is mediated by a combination of passive diffusion, electrophoresis, and electroosmosis due to electrical force acting upon the net negative charge of CFP10pep at neutral pH and/or due to the momentum produced by ion flux through the nanopore [40–43]. The observed preference for αHL nanopore *trans* interactions with CFP10pep, which are not matched by *cis* interactions when the volatage polarity is inverted, suggests this effect is due to the structure or sequence of the target peptide and its specific interactions with the *trans* αHL pore channel or its adjacent surface regions. A nanopore analysis of a 1.5 μM CFP10pep sample under optimized conditions (Fig. 2b–c) to define the criteria for characteristic CFP10pep signal (see methods) detected an − 99.26 pA open pore current (I_0) and a − 38.87 pA characteristic CFP10pep-nanopore interaction current (I_1), each of which had a Gaussian distribution (Fig. 2d–e). To define the characteristic dwell time of a CFP10pep interaction with the αHL nanopore, all signal events that were not excluded by the mean $I_0 + 5 \times$ SD [blank] threshold were split by the percent time (< 50 % and ≥50 %) their current amplitude fell within the window defined for CFP10pep events ($I_1 \pm$ SD [blank], Fig. 2f). The area under the receiver operating characteristic (AUROC) curve analysis of this data (Fig. 2g) revealed a 0.95 probability to distinguish these groups, and determined that a 0.25 ms dwell time threshold produced the maximum sum of specificity and specificity (84.6 % and 92.8 %, respectively). Characteristic CFP10pep peaks were thus required to produce current amplitudes that fell within the pre-defined $I_1 \pm$ SD [blank] window and dwell times > 0.25 ms. CFP10pep signal defined by these criteria accounted for 57 % of all nanopore interaction events detected from a validation sample, yielded a CFP10pep on rate (K_{on}) of 19.3 ± 2.4 events/(min × μM), and was highly distinct from non-specific interactions likely resulting from current spikes due to transient occlusion of the nanopore. Spontaneous gating events detected in the absence of CFP10pep peptide are negligible and would not fit the selection criteria for characteristic αHL nanopore CFP10pep peptide signal (Fig. S4).

Sensitivity and specificity of αHL-mediated CFP10pep detection

To determine the analytical performance of an CFP-10pep αHLN readout, we employed nanopore analysis using aliquots spiked with serial dilutions of synthetic CFP-10pep (Fig. 2g,h). The CFP10pep detection rate revealed a strong linear response with CFP10pep

concentration (R^2 = 0.98) from 0.5 to 5000 pM, where the correspondence between the frequency of CFP10pep signature events [f sig (min^{-1})] and CFP10pep concentration was defined by the equation 0.3412 × $\log_{10}$ [CFP10pep (pM)] - 0.6342 in this analysis.

To evaluate the sequence specificity of the αHL signal characteristics produced upon CFP10pep interaction with the *trans* face of αHL, we analyzed the αHL signals produced under reducing conditions upon αHL *trans* exposure to CFP10pep and a sequence variant containing an additional N-terminal residue (CFP10pepC). These two peptides each demonstrated highly distinctive characteristic αHL signals (Fig. 3), with CFP10pepC more effectively blocking the αHL open pore current than CFP10pep (91.46 pA vs. 60.93 pA decrease) and having a greater αHL dwell time (6.93 ms vs. 0.90 ms), while also revealing a decreased αHL association rate (4.66 ± 1.3 vs. 19.48 ± 2.5 min^{-1} *μM^{-1}). Similarly, modification of CFP10pep by terminal addition of other amino acids produced distinct pore interaction signatures that revealed characteristic differences in αHL blockade currents, dwell times, or association rates (Fig. S5). These results thus expand upon those of a previous study that reported that aerolysin nanopores could distinguish different length polyarginine peptides by their distinctive blockade currents and dwell times [22].

CFP10pep enrichment and detection from trypsin-digested serum samples

To assess the performance of the complete αHL-read CFP10pep IP-NP assay with serum samples, healthy human serum was spiked with recombinant CFP-10 protein, then trypsin digested and immunoprecipitated, after which captured peptides were eluted and analyzed following addition to the *trans* well of an αHL readout device. Nanopore analysis of these samples resulted in frequent and prolonged pore blockades and unstable current baselines (Fig. 4a). This appeared to result from lipid or lipoprotein complexes that were non-specifically adsorbed by the immunoprecipitation matrix and released during peptide elution to block the αHL channel or destabilize its lipid bilayer during peptide analysis, since this blockage rate was markedly reduced when samples were lipid extracted before immunoprecipitation. Treatment of digested serum samples with two commercial lipid removal agents revealed variable effectiveness in reducing these artifacts, with one reagent (LRA; synthetic calcium silicate hydrate) revealing little to no effect to reduce the frequency, duration, and extent of non-specific pore blockages. Serum digests treated with the second reagent demonstrated the absence of these artifacts, although samples required an extended incubation step to reduce a high background of non-specific transient current spikes observed after shorter incubation (Fig. 4a: 10 min vs. 2.5 min), which we hypothesized derived from trace levels of lipid-associated peptides or proteins not fully removed by the shorter incubation period. CFP-10pep αHL signals detected from serum CFP10pep immunoprecipitates following effective lipid-depletion revealed blockade current and dwell time characteristics similar to those observed with synthetic CFP10pep standards or CFP10pep immunoprecipitates captured from PBS suspensions (Fig. 2c), and were not influenced by several factors responsible for clinical interferences (Fig. S6). Similar results were also found upon αHL analysis of a CFP10pep immunoprecipitate isolated from the lipid-depleted and trypsin-digested serum of a TB patient, which detected a mix of non-specific and CFP10pep-specific αHL signal events (Fig. 4b–c), with the latter events exhibiting core blockade current and dwell time values similar to those determined with

synthetic peptide and CFP10pep immunoprecipitates of CFP-10 spiked healthy human serum digests.

These serum processing and αHL readout conditions were next employed to analyze CFP10pep signal from serum samples drawn from individuals with and without TB, using the frequency αHL signaling events that matched the characteristics of CFP10pep detection to establish a background for spontaneous signals arising from chance. This threshold was set at the mean signal frequency in a healthy serum sample plus three times the standard deviation, based on the estimate that only ~0.15 % of random signal consistent with αHL should fall above this range, assuming that the frequency of such false-positive signal follows a normal distribution. This threshold correctly classified all four individuals who did not have TB as being TB-negative based on their serum CFP10pep signal frequency (Fig. 4d). It also detected positive and negative CFP10pep results for serum collected from TB patients at one month and one year after anti-TB treatment initiation, respectively, as would be expected given the known rate of TB resolution at these time frames.

Conclusion

Our results indicate that our described target biomarker peptide selection and IP-NP assay approach can be employed to detect disease-specific biomarkers generated upon trypsin digestion of complex biological samples. In this study, our approach identified a nanopore biomarker target suitable for IP and nanopore detection, which was sensitively detected at the sub-picomolar range in analytical validation studies. This workflow, from target selection through signal readout should be readily adapted to identify and quantify peptides associated with other infectious or malignant diseases for which specific biomarker sequences are known. Such target peptides must produce characteristic signals, but the specific interactions that produce these signals do not need to be known. We therefore envision this approach can represent a viable alternative to targeted mass spectrometry for peptide-based diagnostic applications, particularly since such assays have the potential to be readily adapted to standalone miniaturized nanopore systems suitable for use in point-of-care-testing at remote and resource-poor areas to improve diagnosis in underserved areas. Such assays would benefit from the development of low volume systems that employ membranes incorporating multiple nanopores, since both these factors would reduce sample analysis times to increase assay throughput.

Supplementary Material

Refer to Web version on PubMed Central for supplementary material.

Acknowledgments

The work was primarily supported by research funding provided by the National Institutes of Health (U01CA214254, R01HD090927, R01AI122932, R01AI113725, R21Al126361-01, R01AI144168 and R21AI154284). All authors read the manuscript and contributed to the manuscript review, revision, and finalization.

References

[1]. Whiting PF, Smidt N, Sterne JA, Harbord R, Burton A, Burke M, Beynon R, Ben-Shlomo Y, Axford J, Dieppe P, Ann. Intern. Med. 152 (2010) 456–464. [PubMed: 20368651]

[2]. Gomara M, Haro I, Curr. Med. Chem. 14 (2007) 531–546. [PubMed: 17346145]

[3]. Stathopoulou E, Routsias J, Stea E, Moutsopoulos H, Tzioufas A, Clin. Exp. Immunol. 141 (2005) 148–154. [PubMed: 15958081]

[4]. Sauna ZE, Kimchi-Sarfaty C, Nat. Rev. Genet. 12 (2011) 683–691. [PubMed: 21878961]

[5]. Sylvester KG, Ling XB, Liu G, Kastenberg ZJ, Ji J, Hu Z, Peng S, Lau K, Abdullah F, Brandt ML, Gut 63 (2014) 1284–1292. [PubMed: 24048736]

[6]. Muller PA, Vousden KH, Nat. Cell Biol. 15 (2013) 2–8. [PubMed: 23263379]

[7]. Yadav M, Jhunjhunwala S, Phung QT, Lupardus P, Tanguay J, Bumbaca S, Franci C, Cheung TK, Fritsche J, Weinschenk T, Nature 515 (2014) 572–576. [PubMed: 25428506]

[8]. Chen C-T, Wagner H, Still WC, Science 279 (1998) 851–853. [PubMed: 9452382]

[9]. Gombart AF, Bhan I, Borregaard N, Tamez H, Camargo CA Jr, Koeffler HP, Thadhani R, Clin. Infect. Dis. 48 (2009) 418–424. [PubMed: 19133797]

[10]. Santagata S, Eberlin LS, Norton I, Calligaris D, Feldman DR, Ide JL, Liu X, Wiley JS, Vestal ML, Ramkissoon SH, Proc. Natl. Acad. Sci. USA 111 (2014) 11121–11126. [PubMed: 24982150]

[11]. Giesen C, Wang HA, Schapiro D, Zivanovic N, Jacobs A, Hattendorf B, Schüffler PJ, Grolimund D, Buhmann JM, Brandt S, Nat. Methods 11 (2014) 417–422. [PubMed: 24584193]

[12]. Sela-Culang I, Ofran Y, Peters B, Curr. Opin. Virol. 11 (2015) 98–102. [PubMed: 25837466]

[13]. Medzihradszky KF, Chalkley RJ, Mass Spectrom. Rev. 34 (2015) 43–63. [PubMed: 25667941]

[14]. Gillette MA, Carr SA, Nat. Methods 10 (2013) 28. [PubMed: 23269374]

[15]. Liebler DC, Zimmerman LJ, Biochemistry 52 (2013) 3797–3806. [PubMed: 23517332]

[16]. Howorka S, Siwy ZS, Nat. Biotechnol. 38 (2020) 159–160. [PubMed: 31974421]

[17]. Shi W, Friedman AK, Baker LA, Anal. Chem. 89 (2017) 157–188. [PubMed: 28105845]

[18]. Deamer D, Akeson M, Branton D, Nat. Biotechnol. 34 (2016) 518–524. [PubMed: 27153285]

[19]. Maitra RD, Kim J, Dunbar WB, Electrophoresis 33 (2012) 3418–3428. [PubMed: 23138639]

[20]. Leggett RM, Clark MD, J. Exp. Bot. 68 (2017) 5419–5429. [PubMed: 28992056]

[21]. Varongchayakul N, Song J, Meller A, Grinstaff MW, Chem. Soc. Rev. 47 (2018) 8512–8524. [PubMed: 30328860]

[22]. Piguet F, Ouldali H, Pastoriza-Gallego M, Manivet P, Pelta J, Oukhaled A, Nat. Commun. 9 (2018) 1–13. [PubMed: 29317637]

[23]. Zhao Q, Jayawardhana DA, Wang D, Guan X, J. Phys. Chem. B 113 (2009) 3572–3578. [PubMed: 19231820]

[24]. Kennedy E, Dong Z, Tennant C, Timp G, Nat. Nanotechnol. 11 (2016) 968–976. [PubMed: 27454878]

[25]. Ren R, Wang X, Cai S, Zhang Y, Korchev Y, Ivanov AP, Edel JB, Small Methods 4 (2020) 2000356.

[26]. Sze JY, Ivanov AP, Cass AE, Edel JB, Nat. Commun. 8 (2017) 1–10. [PubMed: 28232747]

[27]. Waduge P, Hu R, Bandarkar P, Yamazaki H, Cressiot B, Zhao Q, Whitford PC, Wanunu M, ACS Nano 11 (2017) 5706–5716. [PubMed: 28471644]

[28]. Rosen CB, Rodriguez-Larrea D, Bayley H, Nat. Biotechnol. 32 (2014) 179–181. [PubMed: 24441471]

[29]. Rotem D, Jayasinghe L, Salichou M, Bayley H, J. Am. Chem. Soc. 134 (2012) 2781–2787. [PubMed: 22229655]

[30]. Wei X, Ma D, Jing L, Wang LY, Wang X, Zhang Z, Lenhart BJ, Yin Y, Wang Q, Liu C, J. Mater. Chem. B 8 (2020) 6792–6797. [PubMed: 32495805]

[31]. Thakur AK, Movileanu L, Nat. Biotechnol. 37 (2019) 96–101.

[32]. Liu C, Lyon C, Bu Y, Deng Z, Walters E, Li Y, Zhang L, Hesseling A, Graviss E, Hu Y, Clin. Chem. 64 (2018) 791–800. [PubMed: 29348166]

[33]. Harding E, Lancet Respir. Med. 8 (2020) 19. [PubMed: 31706931]

[34]. Garrido-Cardenas J, de Lamo-Sevilla C, Cabezas-Fernández M, Manzano-Agugliaro F, Martínez-Lirola M, Tuberculosis (2020) 101917. [PubMed: 32279873]

[35]. Renshaw PS, Panagiotidou P, Whelan A, Gordon SV, Hewinson RG, Williamson RA, Carr MD, J. Biol. Chem. 277 (2002) 21598–21603. [PubMed: 11940590]

[36]. Liu C, Zhao Z, Fan J, Lyon CJ, Wu H-J, Nedelkov D, Zelazny AM, Olivier KN, Cazares LH, Holland SM, Proc. Natl. Acad. Sci. USA 114 (2017) 3969–3974. [PubMed: 28348223]

[37]. Sigal GB, Pinter A, Lowary TL, Kawasaki M, Li A, Mathew A, Tsionsky M, Zheng RB, Plisova T, Shen K, J. Clin. Microbiol. 56 (2018).

[38]. Sutherland TC, Long Y-T, Stefureac R-I, Bediako-Amoa I, Kraatz H-B, Lee JS, Nano Lett. 4 (2004) 1273–1277.

[39]. Chavis AE, Brady KT, Hatmaker GA, Angevine CE, Kothalawala N, Dass A, Robertson JW, Reiner JE, ACS Sens. 2 (2017) 1319–1328. [PubMed: 28812356]

[40]. Boukhet M, Piguet F, Ouldali H, Pastoriza-Gallego M, Pelta J, Oukhaled A, Nanoscale 8 (2016) 18352–18359. [PubMed: 27762420]

[41]. Huang G, Willems K, Soskine M, Wloka C, Maglia G, Nat. Commun. 8 (2017) 1–11. [PubMed: 28232747]

[42]. Wang Y, Tian K, Du X, Shi R-C, Gu L-Q, Anal. Chem. 89 (2017) 13039–13043. [PubMed: 29183111]

[43]. Piguet F, Discala F, Breton M-F, Pelta J, Bacri L, Oukhaled A, J. Phys. Chem. Lett. 5 (2014) 4362–4367. [PubMed: 26273988]

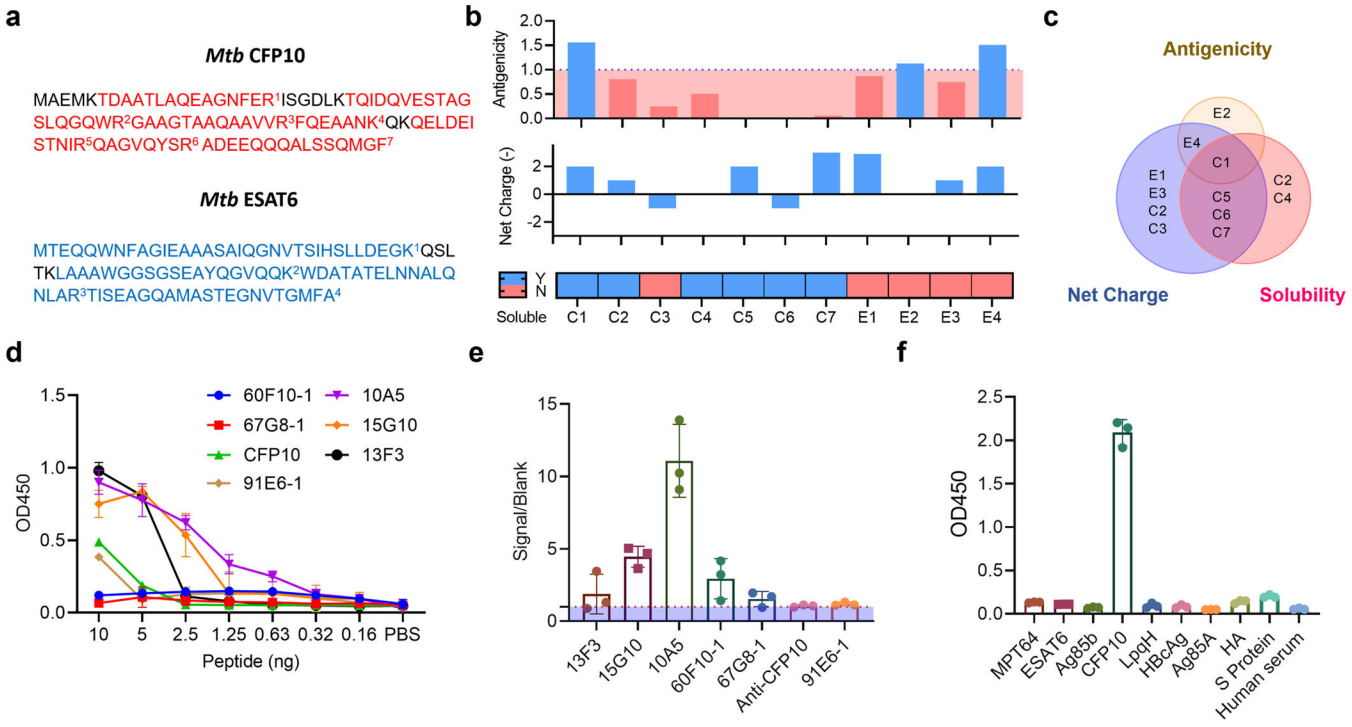

Fig. 1.

Selection of CFP-10 and ESAT-6 peptide targets for antibody enrichment prior to αHL analysis. (a) The sequence of CFP-10 and ESAT-6 indicates all tryptic peptides ≥ 7 amino acids. (b) Predicted antigenicity, net charge and water solubility of all candidate CFP-10 and ESAT-6 target peptides. Blue columns or boxes indicate peptides that meet the criteria for a specified parameter. (c) Venn-diagram of peptides meeting specific criteria for nanopore readout peptides. (d) The signal from an indirect ELISA performed in 10 % healthy human serum to evaluate the relative binding affinity of 0.16–10 ng of the indicated CFP10pep-specific monoclonal antibodies against a CFP10pep serial dilution curve (100–0 ng/mL). (e) Signal-to-blank ratio detected in indirect ELISA performed in 10 % healthy human serum with 10 ng/mL bound CFP10pep and 1 ng of CFP10pep-specific or CFP-10-specific antibody. Data points shown indicate the mean ± SD of triplicate technical replicates for each indicated sample. (f) ELISA results trypsin digests of *Mtb* proteins (MPT64, ESAT6, Ag85b, LpqH, Ag85A), pathogens from other human pathogens (Hepatitis B core protein (HbcAg), Influenza hemagglutinin (HA), SARS-COV-2 S protein), and a pooled healthy donor serum sample (10 ug/mL total protein each).

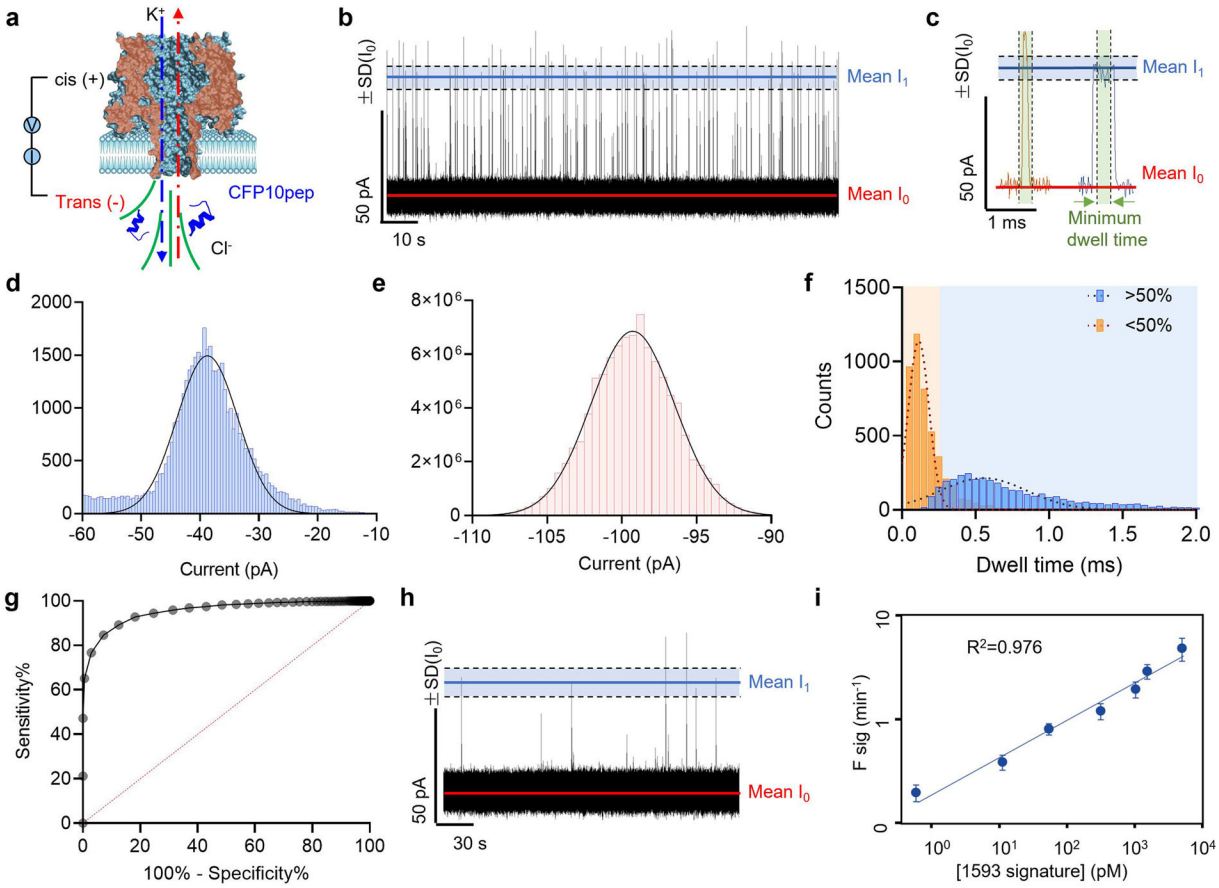

Fig. 2.

Detection of CFP10pep using a αHL nanopore readout system. (a) CFP10pep *trans* capture by the αHL nanopore is driven by peptide electrophoresis and/or electro-osmotic flow resulting from ion movement under negative voltage. (b) A representative single-channel current trace of synthetic CFP10pep *trans* capture (1.5 μM CFP10pep, 4 M KCl, pH 7, and −130 mV), indicating the mean open pore current (99.26 pA; I_0), a characteristic CFP10pep:nanopore interaction signal (38.87 pA; I_1), and zero current (0 pA; dashed green line). (c) Expanded view depicting characteristic nanopore signals caused by non-specific (orange) and CFP10pep-specific (blue) interactions, where CFP10pep nanopore signatures are defined by a characteristic current amplitude and duration of current blockade. (d-e) Current distribution histograms and fitted Gaussian distributions (black lines) of the (d) CFP10pep: nanopore interaction signal (I_1; blue, d) and (e) open-pore signal (I_0, red). (f) Dwell time distribution histograms and fitted Gaussian distributions (dashed lines) for current events that had < 50 % (orange) and ≥ 50 % (blue) of their signal fall within the characteristic CFP10pep current amplitude range (I_1 ± SD [blank]). (g) Area under the receiver operating characteristic (AUROC) graph for the probability of a dwell time threshold to distinguish these events. (h) Representative single-channel current trace of synthetic CFP10pep *trans* capture (50 pM CFP10pep, 4 M KCl, pH 7, and −130 mV). (**i**) Standard curve of the frequency of αHL CFP10pep *trans* capture signatures (F sig) obtained using synthetic CFP10pep concentration standards (0.5–5000 pM). Data points indicate the mean ± SD of triplicate technical replicates for each dilution standard.

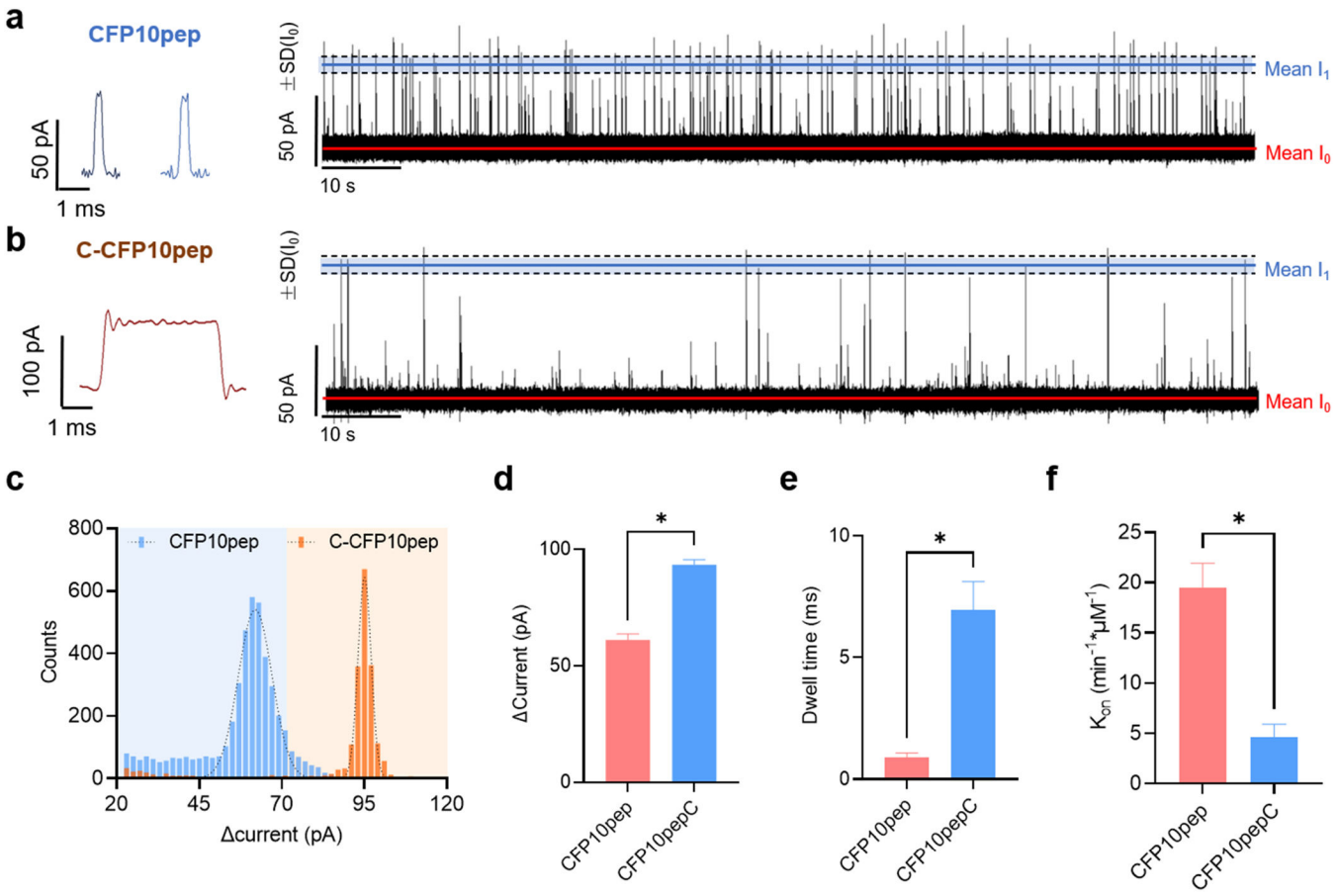

Fig. 3.

Evaluation of the sequence specificity of the αHL CFP10pep interaction signal. (a-b) Representative single-channel current traces for CFP10pep and cystine terminated CFP10pep synthetic peptides produced upon their *trans* capture (1.5 μM target peptide, 4 M KCl and −130 mV), with expanded views depicting characteristic current traces produced by each peptide (left), with scale bars shown below each trace. (c) Current distribution histogram and fitted Gaussian distribution (dashed line) of αHL nanopore CFP10pep and CFP10pep-C signals (1.5 μM target peptide, 4 M KCl, pH 7, and −130 mV). (d–f) Sequence-specific differences in αHL (d) blockade current, (e) dwell time, and (f) peptide on rate determined with an αHL system incubated in *trans* with peptide immune precipitates from trypsin digested healthy human serum samples spiked with synthetic CFP10pep or synthetic CFP10pep modified with an N-terminal cysteine residue (CFP10pepC). Data points denote the mean ± SD values of triplicate technical replicates for each sample, where * indicate p-values < 0.05 and < 0.01 as determined by Mann-Whitney U-tests.

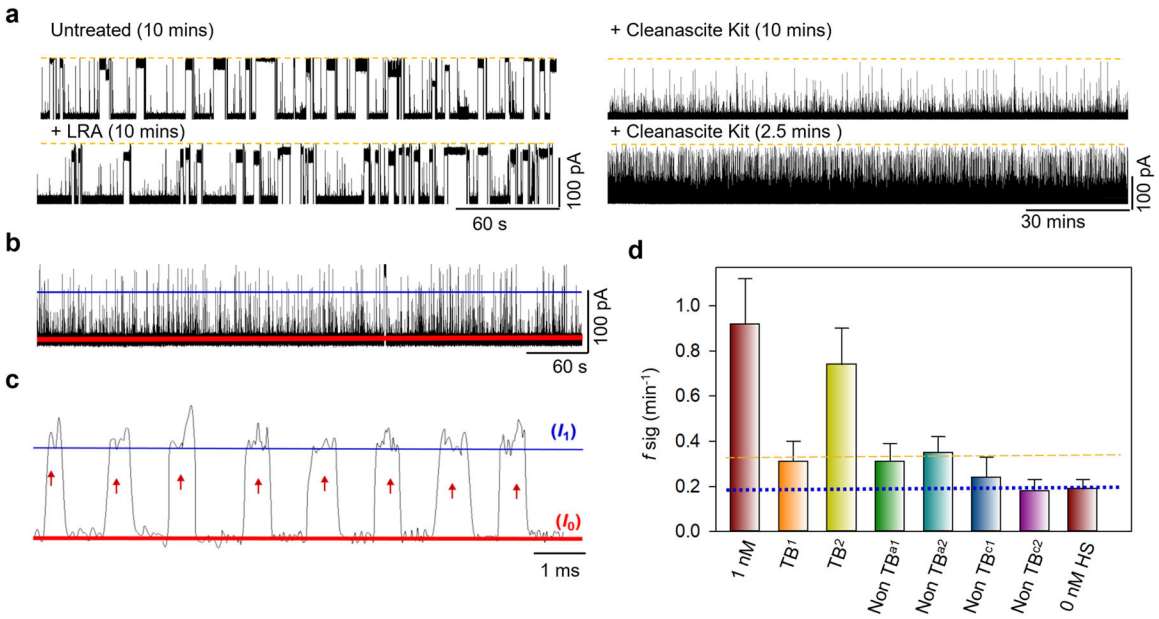

Fig. 4.

CFP10pep detection by αHL analysis of CFP-10-spiked and TB patient serum samples. (a) αHL traces generated with immunoprecipitates of CFP-10 spiked and trypsin-digested healthy human serum samples after treatment with or without LRA or Cleanascite lipid removal reagents. (b) IP-NP assay signal from the trypsin-digested serum of a patient with culture-confirmed TB, and (c) an expanded graph depicting discrete examples of characteristic C1 peptide signatures events detected in this sample. Scale bars are shown below each current trace. (d) CFP10pep IP-NP signal from trypsin-digests of positive and negative control serum samples (1 nM and 0 nM CFP-10-spiked healthy serum), serum from TB patients on short- versus long-term anti-TB treatment (1 month vs. 1 year), and serum from two adults (Non TB^{a}) and two children (Non TB^{c}) without any evidence of TB. Data shown indicate the mean ± SD values of triplicate technical replicates for each dilution standard.

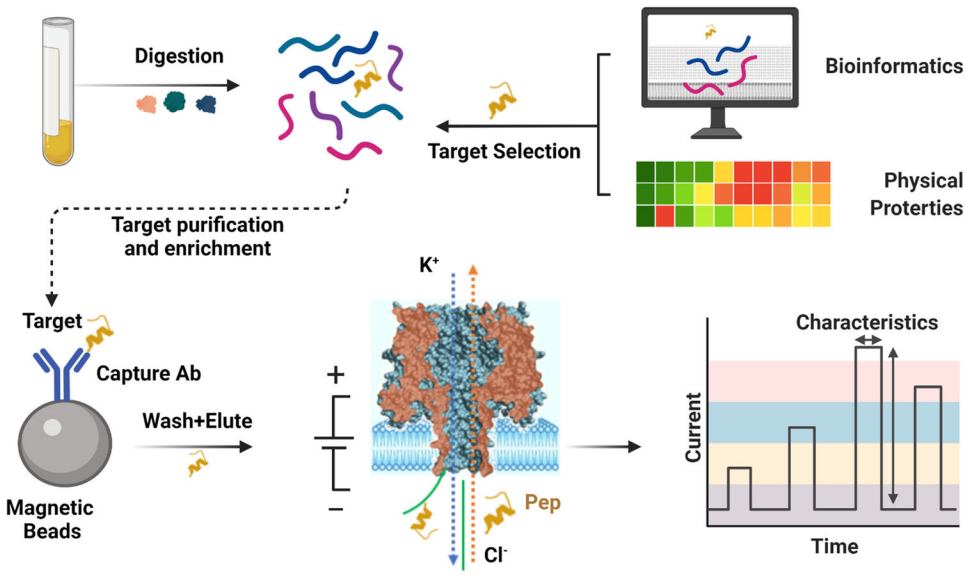

Scheme 1.

Immunoprecipitation nanopore (IP-NP) workflow. Clinical specimens are digested to liberate a biomarker peptide selected based on its bioinformatic and physical properties. This peptide is IP-enriched by binding to a specific antibody bound to a magnetic bead matrix, then washed and added to the *cis* or *trans* side of an αHL nanopore assay chamber. Current signatures induced by the interaction of this peptide at either pore side under varying buffer conditions are analyzed to determine the assay conditions that produce characteristic interaction signals with the highest relative frequency. The frequency of peptide-specific current signatures produced by a standard dilution curve are then used to determine the concentration of the target peptide in analyzed clinical specimens.